

Multiple Majorana zero modes in atomic Fermi double wires with spin-orbit couplingLiang-Liang Wang,¹ Ming Gong,^{2,3} and W.-M. Liu^{1,*}¹*Beijing National Laboratory for Condensed Matter Physics, Institute of Physics, Chinese Academy of Sciences, Beijing 100190, People's Republic of China*²*CAS Key Lab of Quantum Information, University of Science and Technology of China, Hefei 230026, People's Republic of China*³*Synergetic Innovation Center of Quantum Information and Quantum Physics, University of Science and Technology of China, Hefei 230026, People's Republic of China*

(Received 26 January 2017; published 28 August 2017)

Majorana zero modes, quasiparticles with non-Abelian statistics, have gained increasing interest for their fundamental role as building blocks in topological quantum computation. Previous studies have mainly focused on two well-separated Majorana zero modes, which could form two degenerate states serving as one nonlocal qubit for fault-tolerant quantum memory. However, creating and manipulating multiple Majorana zero modes, which could encode more qubits, remain an ongoing research topic. Here we report that multiple Majorana zero modes can exist in atomic Fermi double wires with spin-orbit coupling and perpendicular Zeeman field. This system belongs to the topological BDI class, thus all the topological superfluids are classified by integer numbers. Especially, diverse topological superfluids can be formed in a trap, where the zero energy modes can be found at the interfaces between different topological superfluids. The structure of these zero energy modes in the trap can be engineered by the trapping potential as well as other system parameters. This system would be a significant step towards utilization of Majorana zero modes in quantum computation.

DOI: [10.1103/PhysRevA.96.023623](https://doi.org/10.1103/PhysRevA.96.023623)**I. INTRODUCTION**

Majorana fermions [1–4], unlike Dirac fermions, are fundamental fermionic particles that are their own antiparticles; mathematically, they can be represented as

$$\gamma = \gamma^\dagger. \quad (1)$$

For all the known particles in the standard model, the neutrino with almost zero energy is most likely to be a Majorana fermion; yet in experiments the direct answer is still far from inconclusive. Nevertheless, this exotic particle can still be simulated using the quasiparticles in condensed-matter physics, in which the zero energy modes in superconductors with particle-hole symmetry naturally satisfy the above self-Hermitian condition. These zero energy modes hereafter throughout this work are called Majorana zero modes (MZMs).

These intriguing MZMs are exotic for their non-Abelian exchange statistics [5], rather than Fermi or Bose statistics [4] and their robustness against local perturbations, thus offering a unique platform in fault tolerant topological quantum computation [6–9], quantum memory [10–14], and quantum random-number generation [15,16]. Therefore in the past several years in condensed-matter physics there have been various theoretical proposals for the realization of these zero energy modes [17–34]. Some are worth mentioning among a growing number of diverse proposals, including one-dimensional semiconductor-superconductor heterostructure based quantum wire [18–24], vortices in a spinless $p + ip$ superconductor [25–28], Moore-Read-type states in the $\nu = 5/2$ fractional quantum Hall effect [29,30], and even one-dimensional Fe chains [31–33]. Especially, the observation of a magnetic-field-induced zero-bias conductance peak in InAs and InSb semiconductor nanowires [35–38], Fe

chains [39], and vortex cores in topological insulator- s -wave superconductor hybrid structure [40–42] provide promising evidences for the realization of these MZMs.

Based on previous proposals with only one band in the spin-orbit coupled system, it triggers a topological phase when the magnitude of the Zeeman field exceeds the critical field [18,19,43],

$$|h| \geq h_c = \sqrt{\Delta^2 + \mu^2}, \quad (2)$$

where μ and Δ are chemical potential and s -wave pairing strength, respectively. In this case the topological index such as the Pfaffian and Chern number are nonzero. Otherwise the system is trivial. A pair of MZMs, say γ_1 and γ_2 , are formed at the two open ends, where γ_1 and γ_2 may localize arbitrarily far apart from one another; consequently two nonlocal fermionic states via $f = (\gamma_1 + i\gamma_2)/2$ could serve as one nonlocal topological qubit for fault-tolerant quantum memory [8–14]. Nevertheless, creating and manipulating multiple MZMs, which would be essential for subsequent braiding experiments to demonstrate its non-Abelian nature, still remain a challenge. Up to date the non-Abelian statistics was only simulated based on photonic qubits in the transverse Ising chains [44]. This greatly limits our ability to realize the topological quantum computation based on these systems.

In this article, we propose and validate a specific experimental setup for the realization of multiple MZMs—one-dimensional Fermi double wires with Raman laser-induced SO coupling [45]. The double wires can be readily created by adding a two-dimensional double-well optical lattice. The atoms in each wire are affected by the same SO coupling induced by the Raman lasers. Meanwhile, the same spin atoms in the two wires are linked with the interwire tunneling. Different from the previous studies [46–51], by tuning the interwire tunneling, we find that the traditional gap-closing condition induced by the collective effect of spin-orbit (SO)

*wliu@iphy.ac.cn

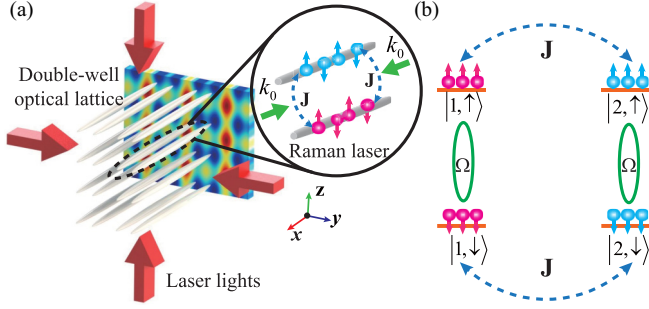


FIG. 1. (a) Schematics diagram for the double-wire system with SO coupling. A double-well optical lattice that has two local minima in a unit cell is formed by the interference of two pairs of counter-propagating laser beams. There is a resulting double-well periodic potential along \hat{z} axis, which allows the interwell tunneling without spin flip. Additionally, two magnetic sublevels $|\uparrow\rangle = |9/2, 9/2\rangle$ and $|\downarrow\rangle = |9/2, 7/2\rangle$ in each wire are coupled by a pair of Raman lasers counterpropagating along \hat{x} axis with the recoil momentum $k_r = k_0 \sin(\theta/2)$, where $k_0 = 2\pi/\lambda$ with λ being the wavelength and $\theta = \pi$ is the angle between two Raman lasers. (b) Effective coupling between four atomic levels $|j, \sigma\rangle$ ($j = 1, 2, \sigma = \uparrow, \downarrow$), where J denotes the interwire tunneling without spin flipping, and Ω represents the intrawire spin-orbit coupling induced by the Raman lasers.

coupling and Zeeman field is shifted and split into two critical transition points $h_{c,1,2} \equiv \sqrt{\Delta^2 + (\mu \pm J)^2}$, where the quasiparticle excitation gap vanishes. As a consequence, phase transitions between different topological regions characterized by (integer) winding numbers can be realized by tuning the chemical potential, Zeeman field, as well as interwire tunneling. We further demonstrate the MZMs within the bulk energy gap by the self-consistent Bogoliubov–de Gennes (BdG) simulations for a cloud trapped in a harmonic potential. These zero modes can be found at the interface between two distinct phases, which is consistent with the local density approximation (LDA). These findings not only provide an splendid platform for exploring multiple MZMs, but also enrich our understanding of topological quantum matters.

II. HAMILTONIAN AND SINGLE-PARTICLE SPECTRUM

The SO coupling for ultracold Fermi atoms has been successfully demonstrated in ultracold ^{40}K and ^6Li gases [52,53], in which the Raman dressing scheme is based on coupling two magnetic sublevels of the ground-state manifold with two counterpropagating Raman lasers [54–65]. The system considered in this work is depicted in Fig. 1(a), where the Raman dressed ^{40}K Fermi gases are loaded in a double-wire geometry, which can be readily realized by adding a two-dimensional double-well optical lattice [66,67]. Note that the optical lattice is spin independent and induces spin-independent tunneling between the coupled wires. We choose the two atomic internal hyperfine states $|9/2, 9/2\rangle$ and $|9/2, 7/2\rangle$ in ^{40}K to label the spin-up ($|j, \uparrow\rangle$) and spin-down ($|j, \downarrow\rangle$) states in both wires for $j = 1, 2$. The atoms move along the \hat{x} axis within a wire and two wires are separated by a distance d in the \hat{z} direction. Moreover, the dynamics along the \hat{y} axis are frozen to the ground states by optical lattice

with high potential depth. The interwire tunneling has the form $J_\sigma = \int dz \psi_{1,\sigma}^*(z)[V(z) \pm \delta]\psi_{2,\sigma}(z)$, where δ denotes the detuning from Raman resonance and $V(z) = c(z^2 - d^2)^2$ with c is the intensity of the laser beams. The positive and negative signs label the detuning to spin-up and spin-down atoms, respectively. We assume them to be real and set $J_\uparrow = J_\downarrow = J$. The four-level topology has been schematically shown in Fig. 1(b), where the blue dashed lines represent the interwire tunneling and the green circles denote the Raman-assisted intrawire interaction with momentum transfer k_r . Four atomic states couple with each other in a cyclic manner with no momentum transferred during a closed-loop transition.

The Hamiltonian is described by $H = \int dx [\mathcal{H}_S + \mathcal{H}_{\text{int}}]$, with the single-particle component \mathcal{H}_S and $\mathcal{H}_{\text{int}} = \sum_{j=1,2} g_j \Psi_{j\uparrow}^\dagger(x) \Psi_{j\downarrow}^\dagger(x) \Psi_{j\downarrow}(x) \Psi_{j\uparrow}(x)$ describing the s -wave contact interaction between the two spin states in the j th wire. The single-particle Hamiltonian is written as

$$\mathcal{H}_S = \sum_{j=1,2} \Psi_j^\dagger(x) \begin{pmatrix} \xi_k + V(x) & \Omega e^{ik_r x} \\ \Omega e^{-ik_r x} & \xi_k + V(x) \end{pmatrix} \Psi_j(x) + J \sum_{\sigma} (\Psi_{1,\sigma}^\dagger(x) \Psi_{2,\sigma}(x) + \text{H.c.}) \quad (3)$$

with $\Psi_j(x) = [\Psi_{j,\uparrow}(x), \Psi_{j,\downarrow}(x)]^T$ being the j th wire atomic annihilation operators, $\xi_k = \epsilon_k - \mu$, where $\epsilon_k = k_x^2/2m$ is the kinetic energy, μ is the chemical potential, m is the mass of an atom, and $V(x)$ is the trapping potential, respectively. The constants Ω and k_r represent the coupling strength and photon recoil momentum of the two-photon Raman coupling, respectively. After applying a local gauge transformation to the above model [68,69], the single-particle Hamiltonian becomes

$$\mathcal{H}_S = \sum_j \Phi_j^\dagger(x) H_0 \Phi_j(x) + J \sum_{\sigma} (\Phi_{1,\sigma}^\dagger(x) \Phi_{2,\sigma}(x) + \text{H.c.}), \quad (4)$$

where the single wire term is $H_0 = \epsilon_k - \mu + V(x) + \alpha k_x \sigma_y - h_z \sigma_z$, with the redefined chemical potential $\mu \rightarrow \mu - E_r/4$ and σ_y, σ_z are the Pauli matrices acting on the spin space.

The effective SO coupling constant $\alpha \equiv E_r/k_r$ and effective Zeeman field $h_z \equiv \Omega$ are introduced. For convenience, the recoil momentum k_r and recoil energy $E_r \equiv k_r^2/2m$ are taken as natural momentum and energy units. Notice that the interaction Hamiltonian \mathcal{H}_{int} is invariant under this gauge transformation [70]. By introducing the interwire tunneling J , the four-band structure of the double-wire system is illustrated in Fig. 2. The spin polarization at the lowest two branches may have different a different sign or the same sign depending strongly on the magnitude of Zeeman field. The same as that in a single-wire system, a perpendicular Zeeman field h_z is required to open an energy gap near the Kramers degenerate point at $k_x = 0$, which is necessary to change the topology of the Fermi surface. As the Zeeman field h_z increases, when $|h_z| > |J|$, an energy gap between the second and third branches is opened, as shown by the red curves in Fig. 2. The dispersion is then built by three energy gaps. Consequently, there would be a topological phase transition when the chemical potential moves from one energy gap to another one.

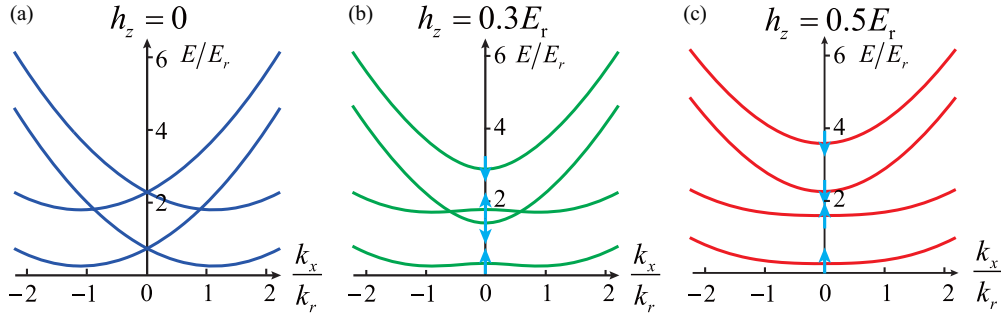


FIG. 2. The evolution of single-particle energy spectra with the increasing of Zeeman field h_z . The band structure is symmetric around $k_x = 0$ in all cases, supporting the superfluids pairing between atoms with opposite momentum. In (a) without Zeeman field, the points at $k_x = 0$ are exactly twofold degenerate due to Kramers's theorem. The energy difference between these two degenerate points are controlled by the interwire tunneling J . In the presence of Zeeman field, this degeneracy is broken, and energy gaps between spin-up and spin-down states [denoted by arrows in (b) and (c)] can be realized. The two lowest bands at $k_x = 0$ may have different spin polarization in moderate Zeeman field (b) or the same spin polarization in the strong Zeeman field limit (c). In all figures, $J = 0.4E_r$ is used.

III. TOPOLOGICAL PHASE DIAGRAMS

To explore in detail the phase transition in the double-wire system, we first consider an infinite homogeneous case with the superfluid pairing formed between atoms in the same wire with opposite momentum $(-k_x, k_x)$. Here we safely neglect the interwire pairings by assuming they are suppressed by the barrier between two wires. Under the Nambu spinor basis $[c_{1\uparrow, k_x}, c_{1\downarrow, k_x}, c_{1\uparrow, -k_x}^\dagger, c_{1\downarrow, -k_x}^\dagger, c_{2\uparrow, k_x}, c_{2\downarrow, k_x}, c_{2\uparrow, -k_x}^\dagger, c_{2\downarrow, -k_x}^\dagger]^T$, the Bogoliubov–de Gennes (BdG) operator in momentum space can be written as

$$H_{\text{BdG}}(k_x) = \begin{pmatrix} H_1(k_x) & \mathcal{J} \\ \mathcal{J}^\dagger & H_2(k_x) \end{pmatrix}, \quad (5)$$

where $\mathcal{J} = \text{diag}(J, J, -J, -J)$ is the interwire tunneling and $H_j(k_x)$ is the Hamiltonian of the j th wire, Δ_j is the pairing order parameter of j th wire, and

$$H_j = \begin{pmatrix} \xi_k - h_z & -i\alpha k_x & 0 & \Delta_j \\ i\alpha k_x & \xi_k + h_z & -\Delta_j & 0 \\ 0 & -\Delta_j^* & -\xi_k + h_z & i\alpha k_x \\ \Delta_j^* & 0 & -i\alpha k_x & -\xi_k - h_z \end{pmatrix}. \quad (6)$$

Here we just consider the symmetric case $\Delta = \Delta_1 = \Delta_2$. We first clarify the topological class of the BdG Hamiltonian $H_{\text{BdG}}(k_x)$ [71]. The representations of the time reversal (Θ), the particle-hole reversal (Σ), and the chiral (S) symmetry are defined as $\Theta = U_T K$, $\Sigma = U_P K$, and $S = \Theta\Sigma = U_S$, where

$$U_T = \rho_0 \otimes \tau_0 \otimes \sigma_0, \quad (7)$$

$$U_P = \rho_0 \otimes \tau_x \otimes \sigma_0, \quad (8)$$

$$U_S = U_T U_P^* = U_P, \quad (9)$$

with ρ , τ , and σ the Pauli matrices acting on double wire space, particle-hole space, and spin space, respectively, K represents the complex conjugate operator and U_T , U_P , and U_S are unitary matrices. It is easy to see that $\Theta^2 = \Sigma^2 = S^2 = 1$, thus the double-wire system belongs to the topological BDI class, which is characterized by the \mathbb{Z} index in one spatial dimension. In order to determine the topological invariant, we then proceed to calculate the winding number W . In general

the BdG Hamiltonian can be transformed into an off-diagonal block form:

$$U^\dagger H_{\text{BdG}}(k_x) U = i \begin{pmatrix} 0 & v(k_x) \\ -v^T(k_x) & 0 \end{pmatrix}, \quad (10)$$

with U the eigenfunctions of U_S [72]. The winding number is then calculated by

$$\begin{aligned} W &\equiv \int \frac{dk_x}{2\pi i} \partial_{k_x} \ln \det v(k_x) = \text{tr} \int \frac{dk_x}{2\pi i} \partial_{k_x} \ln v(k_x) \\ &= \sum_n \int \frac{dk_x}{2\pi i} \partial_{k_x} \ln z_n(k_x) \in \mathbb{Z}, \end{aligned} \quad (11)$$

with $z_n(k_x)$ being the eigenvalues of $v(k_x)$, which are complex values due to the non-Hermiticity of $v(k_x)$.

The phase diagrams are presented in Fig. 3 with the phase boundaries determined by $\det v(k_x) = 0$. Furthermore, we calculate the energy gap E_g at zero momentum and obtain the gap close condition:

$$h_z = \sqrt{\Delta^2 + (J \pm \mu)^2}. \quad (12)$$

If there is no tunneling between the two wires, the critical Zeeman field reduces to the well-known boundary in Eq. (2). It is clearly indicated that the interwire tunneling J directly split the critical point into two critical Zeeman fields: $h_{c1} = \sqrt{\Delta^2 + (J + \mu)^2}$, $h_{c2} = \sqrt{\Delta^2 + (J - \mu)^2}$. The excitation gap vanishes at these two critical values, which represents a topological phase transition. As shown in Fig. 3(a), there is a phase transition from normal to topological state with $W = 1$ when the Zeeman field equals h_{c2} . Furthermore, such topological state ($W = 1$) would undergo a transition to the topological state with $W = 2$ as the Zeeman field is increased to h_{c1} . The colors ranging from dark to red give the value of the energy gap E_g . The phase boundaries using these two criteria are consistent as shown in Fig. 3. In Fig. 3(b), as anticipated in single-particle spectrum, the double-wire system can be in different topological states if the chemical potential is situated within different energy gaps. One can see that the topological phase with $W = 1$ emerges when the chemical potential enters the first and third energy gap, indicating the same topology for two energy gaps. On the other hand, the $W = 2$ state has also been observed as the chemical potential shift to

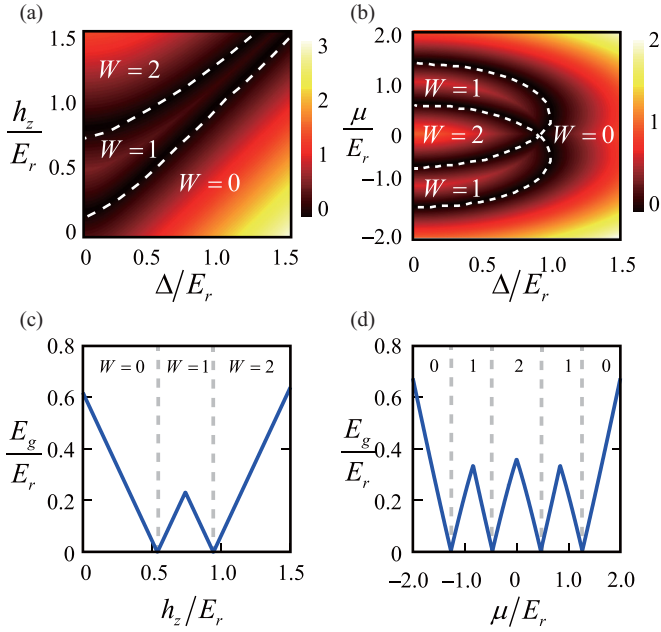


FIG. 3. Topological phase diagrams with the energy gap E_g are shown in (a) $(\Delta-h_z)$ plane with $\mu/E_r = 0.5$, $J/E_r = 0.3$ and (b) $(\Delta-\mu)$ plane with $h_z/E_r = 1.0$, $J/E_r = 0.4$. The colors ranging from dark to red describe the values of E_g and the white dotted lines represent phase boundaries where the energy gap equals zero. (c) The energy gap E_g is plotted with respect to the Zeeman field h_z . There is a jump in the winding number, occurring precisely at $E_g = 0$. Here, the other parameters are chosen as $\Delta/E_r = 0.5$, $J/E_r = 0.3$, and $\mu/E_r = 0.5$. (d) Plot of the energy gap E_g as a function of the chemical potential μ with $\Delta/E_r = 0.5$, $h_z/E_r = 1.0$, and $J/E_r = 0.4$.

the second energy gap. It is noteworthy that by increasing the pairing order parameter Δ , the area of $W = 2$ along the chemical potential gets smaller and finally disappears above the threshold, $\sqrt{h_z^2 - J^2}$, and the trivial phase $W = 0$ will occur for the whole chemical potential space if we move on and reach the limit $h_z^2 - \Delta^2 = 0$. Thus with the introduced interwire tunneling the required minimal Zeeman field may be relaxed from $\sqrt{\mu^2 + \Delta^2}$ to Δ .

These phase transitions can be understood from the viewpoint of gap closing and reopening [see Figs. 3(c) and 3(d)], which is characterized by the energy gap E_g at zero momentum. We find that during the topological phase transitions the gap will be closed and reopened. These transitions can be more precisely understood from the viewpoint of winding number as shown in Fig. 4. We find that in the trivial phase regime, the winding number around the origin is zero when $h_z = 0$, and will enclose the origin by one time when $W = 1$ and two times when $W = 2$. The topological phase transitions in the winding number is determined by $v(k_x) = 0$, in which the gap is closed and reopened since $\det(H_{\text{BdG}}(k_x = 0)) = 0$. We will also show in the following section the realization of MZMs in these topological phases from the bulk-edge correspondence point of view.

IV. MULTIPLE MAJORANA ZERO MODES IN THE HARMONIC TRAP

We now turn to discuss the double-wire system within a harmonic trapping potential $V(x) = m\omega^2 x^2/2$. According to the local-density approximation, the chemical potential can be thought of as a position dependent function, $\mu(x) = \mu - V(x)$, that continuously decreases away from the center of the trap. Therefore, the critical Zeeman field can be accordingly redefined as $h_c(x) = \sqrt{\Delta(x)^2 + [J \pm \mu(x)]^2}$. We start from the case when $\mu(0) > \sqrt{J^2 + h_z^2}$ and $|h_z| > |J|$, thus in the single-particle picture all four bands are occupied [see Fig. 5(a)], in which case the center of the trap is trivial. From the center of the trap to the two wings the topological indexes in the LDA sense are $W = 0, 1, 2, 1, 0$, respectively. With the decreasing of total number of particles, which controls the chemical potential $\mu(0)$, the center of the trap will enter the topological phase regime with $W = 1$ when three bands [Fig. 5(b)], and $W = 2$ when two bands [Fig. 5(c)], are occupied. The corresponding topological number patterns will also be changed accordingly. Due to the smooth profile of chemical potential and order parameters, we find that at the interface between two topological superfluids the change of topological number is at most equal to 1 [the jump by 2 is possible only when $\mu(x) = 0$ is encountered, as can be seen

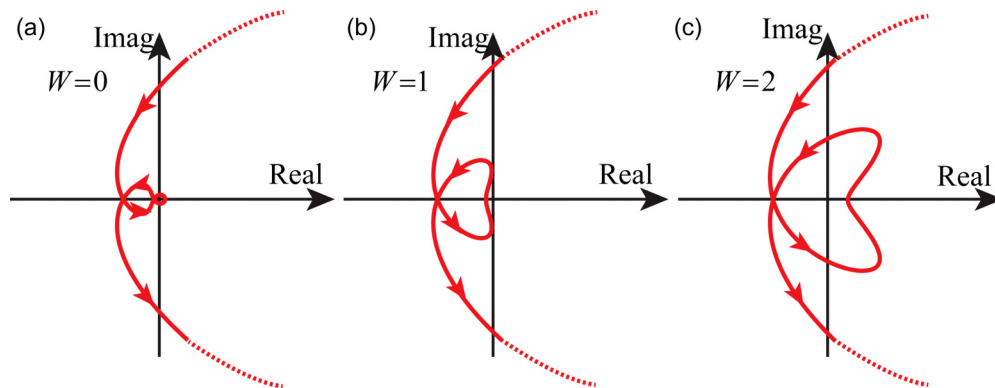


FIG. 4. The curves of $\det v(k_x)$ in the complex space for different Zeeman fields: (a) $h_z = 0$, (b) $h_z/E_r = 0.5$, and (c) $h_z/E_r = 1.2$. In (a) the winding number $W = 0$ since the curve travels counterclockwise first and then clockwise around the origin. Panels (b) and (c) represent the case of $W = 1$ and $W = 2$, respectively. Notice that the two limits $k_x \rightarrow \pm\infty$ will correspond to the same point from the winding number formula (11). Other parameters are $\mu/E_r = 0.5$, $J/E_r = 0.3$, $\Delta/E_r = 0.5$.

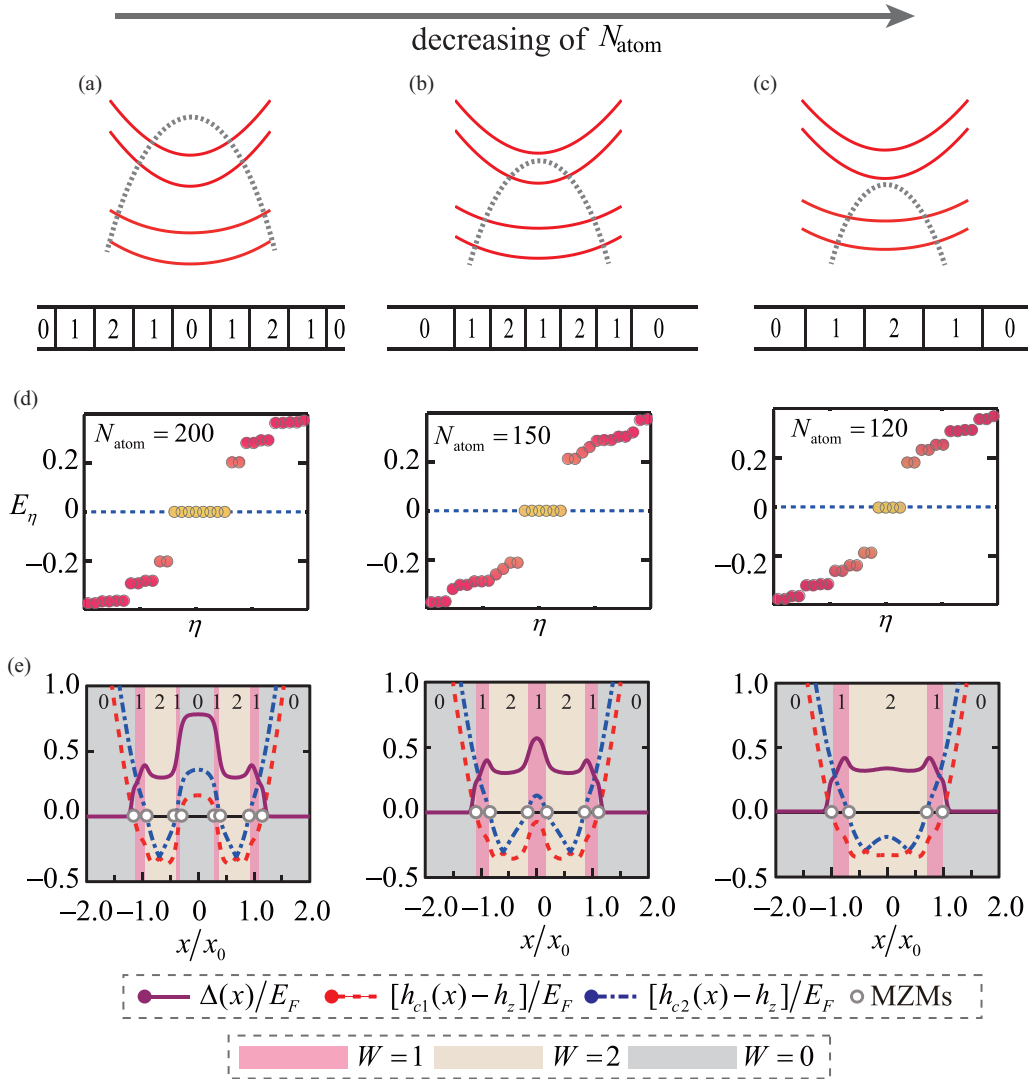


FIG. 5. Topological phases in a trap. Panels (a)–(c) give a rough configuration of the double-wire system in a weak harmonic trap for different total atomic numbers within the local-density approximation. The dot lines give the local chemical potential $\mu(x) = \mu - V(x)$. We start at the point where the total atomic number is set to be large enough that all four bands are occupied. From the center of the trap to the two wings the topological indexes in the LDA sense are $W = 0, 1, 2, 1, 0$, respectively. If we decrease N_{atom} , fewer bands are occupied and fewer topological phases can be distinguished. (d) Quasiparticle excitation spectrum E_η (in units of E_F), calculated within the self-consistent BdG approach, at three total atomic numbers, $N_{\text{atom}} = 200, 150$, and 120 , respectively. Here $\gamma = \pi$, $h_z/E_F = 0.7$, and $J/E_F = 0.2$ (where $E_F = N_{\text{atom}}/4\hbar\omega$ is the Fermi energy). The number of Majorana zero modes changes as the total number of atoms varies, therefore we detect 8, 6, and 4 MZMs, corresponding to the spatial Zeeman fields $[h_{c1}(x) - h_z]$, $[h_{c2}(x) - h_z]$, and the order parameter $\Delta(x)$ shown in (e). The phases distinguished by the winding number are highlighted with different colors. The dots in each subgraph label MZMs associated with interfaces between different phases, where the Zeeman field crosses the lines. It is convenient to use the Thomas-Fermi radius $x_0 = \sqrt{N_{\text{atom}}/4m\omega}$ as the unit of length.

from Fig. 3(b)]. It should be emphasized that the topological number pattern is relatively stable and is almost independent of the external potential.

We further use the exact numerical method to verify the above picture by self-consistently solving the BdG equation in real space, following the method in Ref. [70]. $\varphi_\eta(x) \equiv [u_{1\uparrow\eta}(x), u_{1\downarrow\eta}(x), u_{2\uparrow\eta}(x), u_{2\downarrow\eta}(x), v_{2\uparrow\eta}(x), v_{2\downarrow\eta}(x), v_{1\uparrow\eta}(x), v_{1\downarrow\eta}(x)]^T$ are the Nambu spinor wave functions corresponding to the quasiparticle excitation energy E_η . The BdG Hamiltonian $H_{\text{BdG}}(x)$ can be transformed from the momentum space Hamiltonian in Eq. (6) via ξ_k replaced by $-(1/2m)\partial^2/\partial x^2 + V(x) - \mu$ for the kinetic energy, αk_x by $-i\alpha\partial/\partial x$ for the SO

coupling, and Δ_j by $\Delta_j(x)$ for the pairing order parameter. Furthermore, the order parameter $\Delta_j(x)$, the chemical potential μ can be determined by the self-consistent equations

$$\begin{aligned} \Delta_j(x) &= -\frac{g_{1D}}{2} \sum_\eta [u_{j\uparrow\eta} v_{j\downarrow\eta}^* f(E_\eta) + u_{j\downarrow\eta} v_{j\uparrow\eta}^* f(-E_\eta)], \\ N &= \int dx \sum_{j,\sigma} n_{j\sigma}(x), \\ n_{j\sigma}(x) &= \frac{1}{2} \sum_\eta [|u_{j\sigma\eta}(x)|^2 f(E_\eta) + |v_{\sigma\eta}(x)|^2 f(-E_\eta)]. \end{aligned} \quad (13)$$

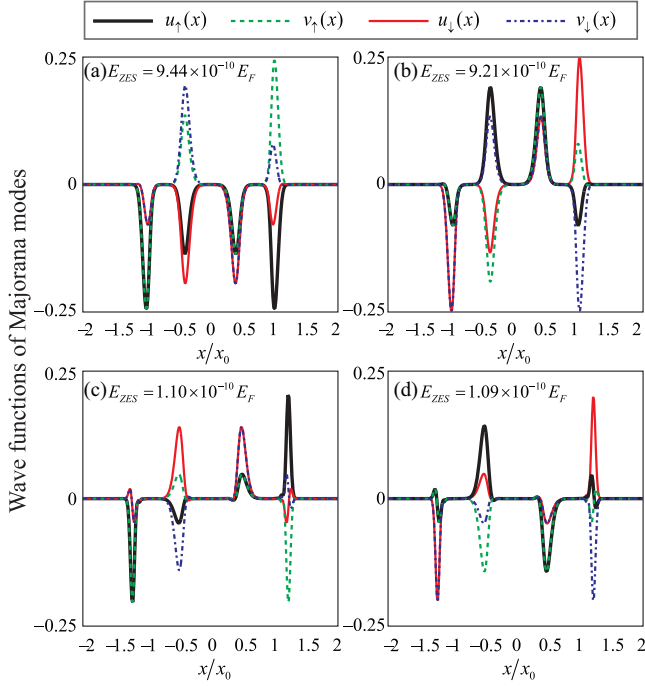


FIG. 6. Wave functions of four paired Majorana zero modes. Due to the intrinsic symmetry $u_{j\sigma\eta}^+(x) = v_{j\sigma\eta}^{-*}(x)$ with $E_\eta \rightarrow -E_\eta$, where \pm refer to quasiparticle and hole excitations, we just show the wave functions of quasiparticle zero modes. All modes satisfy the symmetry requirement for Majorana wave function $u_\sigma(x) = v_\sigma^*(x)$ or $u_\sigma(x) = -v_\sigma^*(x)$ [here $u_\sigma(x) = u_{1\sigma}(x) = u_{2\sigma}(x)$, $v_\sigma(x) = v_{1\sigma}(x) = v_{2\sigma}(x)$]. The parameters are the same as the case in Fig. 5 with $N_{\text{atom}} = 200$.

Here $n_{j\sigma}$ is the local density of fermions in j -th wire with spin σ , and $f(x) = 1/(1 + e^{x/k_B T})$ is the quasiparticle Fermi-Dirac distribution at the temperature T . The harmonic basis up to 400 harmonic oscillators are used to construct the eigenfunctions, which is found to be large enough to ensure the numerical accuracy. Moreover, the dimensionless interaction parameter $\gamma \equiv -mg_{1D}/n_0$ is used to characterize the interaction strength, where n_0 is the zero-temperature center density of ideal fermionic gases.

Figure 5(d) show the mean-field energy spectrum with different total particle numbers. The emergence of MZMs can be clearly revealed by the behavior of the energy spectrum. At a large total particle number $N_{\text{atom}} = 200$, eight quasiparticle modes with nearly zero energy are clearly spectrally separated from all other states. Furthermore, we observe six Majorana zero energy modes with $N_{\text{atom}} = 150$ and four MZMs with $N_{\text{atom}} = 120$, corresponding to what we have discussed in Figs. 5(a)–5(c). As predicted within the LDA, the number of MZMs changes as the total number of atoms decreases. The corresponding calculation of $[h_{c,1,2}(x) - h_z]$ for a local uniform cell at position x with the local chemical potential $\mu(x)$ and order parameter $\Delta(x)$ [in this case, $\Delta(x) = \Delta_1(x) = \Delta_2(x)$] are given in Fig. 5(e). The symmetry around the \hat{x} axis originates from the harmonic trapping geometry. Zero-energy modes, labeled with white dots, just locate around the place $h_z = \sqrt{\Delta(x)^2 + [J \pm \mu(x)]^2}$, corresponding to the steep slope of the order parameter. For example, at a total particle number $N_{\text{atom}} = 200$, the trivial phase takes over the central region of the system and six nontrivial topological districts are detected in the trap. This suggests that there are eight phase transition

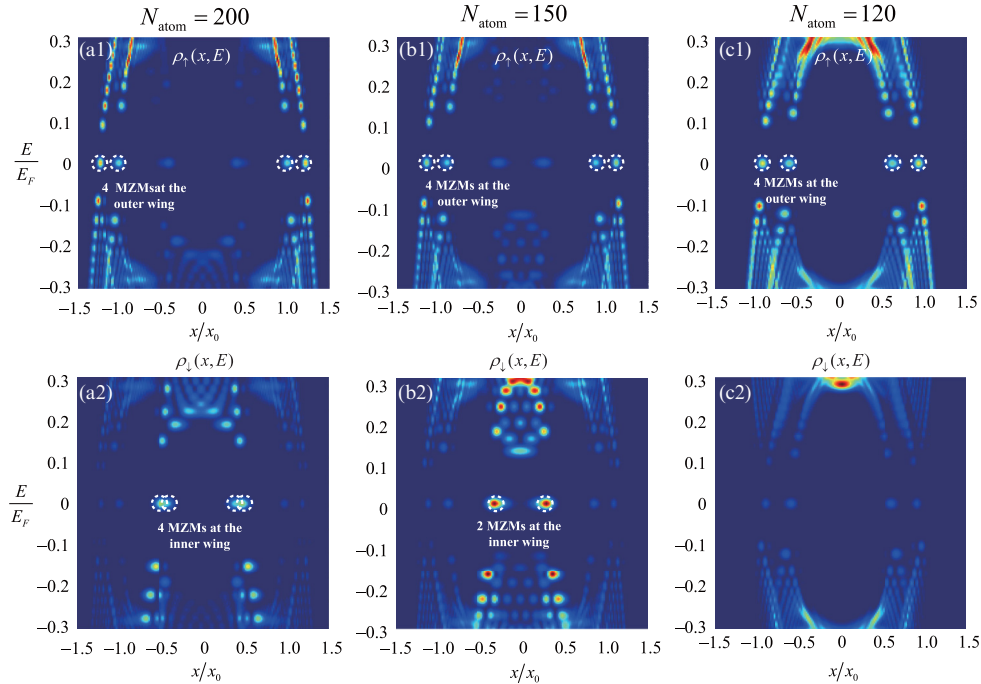


FIG. 7. Linear contour plot for the local density of states of spin-up atoms $\rho_\uparrow(x, E)$ and of spin-down atoms $\rho_\downarrow(x, E)$ with different total atom number: (a) $N_{\text{atom}} = 200$, (b) $N_{\text{atom}} = 150$, and (c) $N_{\text{atom}} = 120$. The signals of MZMs are well isolated in the energy domain and real space, and highlighted by white circles. (a) Eight MZMs are well localized at $x \simeq \pm 1.2x_0$, $x \simeq \pm 1.0x_0$, $x \simeq \pm 0.5x_0$, and $x \simeq \pm 0.4x_0$. (b) Six Majorana zero modes are well localized at $x \simeq \pm 1.2x_0$, $x \simeq \pm 1.0x_0$, and $x \simeq \pm 0.3x_0$. (c) Four Majorana zero modes are well localized at $x \simeq \pm 0.8x_0$ and $x \simeq \pm 0.5x_0$.

points over the whole system, therefore we detect eight MZMs associated with interfaces between different phases, where the spatial Zeeman field $h_z(x) = \sqrt{\Delta(x)^2 + [J \pm \mu(x)]^2}$ equals zero. It is obvious that fewer MZMs remain if we further decrease the total number of particle N_{atom} . The trivial area at the trap center gets shrunk and eventually disappears at about $N_{\text{atom}} \sim 170$, and only six MZMs are preserved. The agreement between BdG and LDA result is excellent and both theories predict the same multiple-shell structures.

Because of the intrinsic symmetry in the BdG formalism, H_{BdG} is invariant under the particle-hole transformation: $E_\eta \rightarrow -E_\eta$, $\gamma_E = \gamma_{-E}^\dagger$. One can immediately find that the zero-energy quasiparticle states satisfy the self-Hermitian condition in Eq. (1), thus these modes can be regarded as Majorana fermions. The corresponding wave functions for these zero-energy states should satisfy either $u_{j\sigma}(x) = v_{j\sigma}^*(x)$ or $u_{j\sigma}(x) = -v_{j\sigma}^*(x)$. The wave functions of the MZMs in Fig. 5(d) are shown in Fig. 6. In a finite size system, the overlap between the wave functions at the two ends lead to finite but exponentially small energy splitting: $E_{\text{ZES}} \approx \pm 9 \times 10^{-10} E_F$. We can see that the wave functions readily satisfy either $u_{j,\sigma}(x) = v_{j,\sigma}^*(x)$ or $u_{j,\sigma}(x) = -v_{j,\sigma}^*(x)$, meeting the requirement of symmetry or antisymmetry. In practice, a direct and convenient way to detect multiple MZMs is using spatially resolved radio-frequency (rf) spectroscopy. It measures spatially localized zero-energy peaks yielded by MZMs in local density of states (LDOS), which are separated from other quasiparticle states. The local density of states for spin-up and spin-down atoms is defined as

$$\rho_\sigma(x, E) = \frac{1}{4} \sum_{j=1,2,\eta} [|u_{j,\sigma,\eta}|^2 \delta(E - E_\eta) + |v_{j,\sigma,\eta}|^2 \delta(E + E_\eta)]. \quad (14)$$

In Fig. 6, we show that the local density of states $\rho_\sigma(x, E)$ and the contribution from MZMs are clearly visible near zero energy and well separated from other quasiparticle contributions by an energy gap $\Delta \sim 0.1 E_F$. There are eight Majorana induced zero-energy peaks localized pairwise at the trap outer wing $x = \pm 1.2 E_F$, $x = \pm 1.0 E_F$ and at the inner wing $x = \pm 0.5 E_F$, $x = \pm 0.4 E_F$ in Fig. 6(a). The two peaks at the inner wing are not distinguishable because of the superposition of the wave functions. In addition, we can clearly

see six (four) Majorana induced signals in Fig. 7(b) [Fig. 7(c)]. It is interesting to note that the Majorana zero-energy modes at the outer wing and inner wing mainly contribute to $\rho_\uparrow(x, E)$ and $\rho_\downarrow(x, E)$, respectively.

V. CONCLUDING REMARKS

We propose a scheme to realize and manipulate multiple MZMs by using atomic Fermi double wires with spin-orbit interaction and investigate the possibly novel topological properties. The tunneling between two wires triggers the separation of previous topological phase region and generates two diverse topological phases, characterized by the winding number, representing a topological property. We give the gap-closing condition to determine the topological phase boundaries and map out the phase diagram for interpreting the emergence of multiple MZMs. In addition, we give the reliable results by solving the self-consistent BdG equation within a harmonic trap and predict that numerous MZMs associated with interfaces between diverse phases depend on not only the combined effect of SO coupling and the Zeeman field, but also the interlayer tunneling, thus offering more knobs in experiments. Experimentally, multiple MZMs can be detected by applying the spatially resolved radio-frequency spectroscopy, which would show a well-isolated signal at zero energy. The atomic Fermi double wires with SO coupling described here not only provide fertile grounds for further experiments to investigate the exotic topological superfluid and associated multiple MZMs, but also constitutes a critical step towards universal quantum computation.

ACKNOWLEDGMENTS

We thank A.-C. Ji and Q. Sun for their early contribution to this project and are grateful to K. A. Yasir and X.-X. Lv for valuable discussions. This work was supported by the NKRD under Grant No. 2016YFA0301500, NSFC under Grants No. 11434015, No. 61227902, No. 61378017, and No. KZ201610005011, SKLQOQOD under Grant No. KF201403, SPRPCAS under Grants No. XDB01020300 and No. XDB21030300. M.G. was supported by the National Youth Thousand Talents Program (Grant No. KJ2030000001), the USTC start-up funding (Grant No. KY2030000053), and the CUHK RGC Grant (Grant No. 401113).

[1] E. Majorana, *Nuovo Cim. (in Italian)* **14**, 171 (1937).
 [2] F. Wilczek, *Nat. Phys.* **5**, 614 (2009).
 [3] P. W. Brouwer, *Science* **336**, 989 (2012).
 [4] S. R. Elliott and M. Franz, *Rev. Mod. Phys.* **87**, 137 (2015).
 [5] D. A. Ivanov, *Phys. Rev. Lett.* **86**, 268 (2001).
 [6] M. Z. Hasan and C. L. Kane, *Rev. Mod. Phys.* **82**, 3045 (2010).
 [7] X. L. Qi and S. C. Zhang, *Rev. Mod. Phys.* **83**, 1057 (2011).
 [8] S. Tewari, S. Das Sarma, C. Nayak, C. Zhang, and P. Zoller, *Phys. Rev. Lett.* **98**, 010506 (2007).
 [9] C. Nayak, S. H. Simon, A. Stern, M. Freedman, and S. D. Sarma, *Rev. Mod. Phys.* **80**, 1083 (2008).
 [10] A. Y. Kitaev, *Phys. Usp.* **44**, 131 (2001).

[11] A. Y. Kitaev, *Ann. Phys.* **303**, 2 (2003).
 [12] P. W. Shor, *Phys. Rev. A* **52**, R2493(R) (1995).
 [13] M. J. Biercuk, H. Uys, A. P. VanDevender, N. Shiga, W. M. Itano, and J. J. Bollinger, *Nature (London)* **458**, 996 (2009).
 [14] P. C. Maurer, G. Kucsko, C. Latta, L. Jiang, N. Y. Yao, S. D. Bennett, F. Pastawski, D. Hunger, N. Chisholm, M. Markham, D. J. Twitchen, J. I. Cirac, and M. D. Lukin, *Science* **336**, 1283 (2012).
 [15] J. G. Rarity, P. C. M. Owens, and P. R. Tapster, *J. Mod. Opt.* **41**, 2435 (1994).
 [16] D.-L. Deng and L.-M. Duan, *Phys. Rev. A* **88**, 012323 (2013).
 [17] J. Alicea, *Rep. Prog. Phys.* **75**, 076501 (2012).

- [18] R. M. Lutchyn, J. D. Sau, and S. Das Sarma, *Phys. Rev. Lett.* **105**, 077001 (2010).
- [19] Y. Oreg, G. Refael, and F. von Oppen, *Phys. Rev. Lett.* **105**, 177002 (2010).
- [20] J. Alicea, Y. Oreg, G. Refael, F. von Oppen, and M. P. A. Fisher, *Nat. Phys.* **7**, 412 (2011).
- [21] E. M. Stoudenmire, J. Alicea, O. A. Starykh, and M. P. A. Fisher, *Phys. Rev. B* **84**, 014503 (2011).
- [22] T. D. Stanescu, R. M. Lutchyn, and S. Das Sarma, *Phys. Rev. B* **84**, 144522 (2011).
- [23] L. Jiang, T. Kitagawa, J. Alicea, A. R. Akhmerov, D. Pekker, G. Refael, J. I. Cirac, E. Demler, M. D. Lukin, and P. Zoller, *Phys. Rev. Lett.* **106**, 220402 (2011).
- [24] A. Bühler, N. Lang, C. V. Kraus, G. Möller, S. D. Huber, and H. P. Büchler, *Nat. Commun.* **5**, 4504 (2014).
- [25] N. Read and D. Green, *Phys. Rev. B* **61**, 10267 (2000).
- [26] T. Mizushima, M. Ichioka, and K. Machida, *Phys. Rev. Lett.* **101**, 150409 (2008).
- [27] K. Björnson and A. M. Black-Schaffer, *Phys. Rev. B* **91**, 214514 (2015).
- [28] J. M. Murray and O. Vafek, *Phys. Rev. B* **92**, 134520 (2015).
- [29] L. Sheng, D. N. Sheng, C. S. Ting, and F. D. M. Haldane, *Phys. Rev. Lett.* **95**, 136602 (2005).
- [30] C. L. Kane and E. J. Mele, *Phys. Rev. Lett.* **95**, 146802 (2005).
- [31] S. Nadj-Perge, I. K. Drozdov, B. A. Bernevig, and A. Yazdani, *Phys. Rev. B* **88**, 020407 (2013).
- [32] J. Li, H. Chen, I. K. Drozdov, A. Yazdani, B. A. Bernevig, and A. H. MacDonald, *Phys. Rev. B* **90**, 235433 (2014).
- [33] R. Pawlak, M. Kisiel, J. Klinovaja, T. Meier, S. Kawai, T. Glatzel, D. Loss, and E. Meyer, *npj Quantum Inf.* **2**, 16035 (2016).
- [34] M. Gong, G. Chen, S. Jia, and C. Zhang, *Phys. Rev. Lett.* **109**, 105302 (2012).
- [35] V. Mourik, K. Zuo, S. M. Frolov, S. R. Plissard, E. P. A. M. Bakkers, and L. P. Kouwenhoven, *Science* **336**, 1003 (2012).
- [36] L. P. Rokhinson, X. Liu, and J. K. Furdyna, *Nat. Phys.* **8**, 795 (2012).
- [37] M. T. Deng, C. L. Yu, G. Y. Huang, M. Larsson, P. Caroff, and H. Q. Xu, *Nano. Lett.* **12**, 6414 (2012).
- [38] A. Das, Y. Ronen, Y. Most, Y. Oreg, M. Heiblum, and H. Shtrikman, *Nat. Phys.* **8**, 887 (2012).
- [39] S. Nadj-Perge, I. K. Drozdov, J. Li, H. Chen, S. Jeon, J. Seo, A. H. MacDonald, B. Andrei Bernevig, and A. Yazdani, *Science* **346**, 602 (2014).
- [40] J.-P. Xu, C. Liu, M.-X. Wang, J. Ge, Z.-L. Liu, X. Yang, Y. Chen, Y. Liu, Z.-A. Xu, C.-L. Gao, D. Qian, F.-C. Zhang, and J.-F. Jia, *Phys. Rev. Lett.* **112**, 217001 (2014).
- [41] J.-P. Xu, M.-X. Wang, Z. L. Liu, J.-F. Ge, X. Yang, C. Liu, Z. A. Xu, D. Guan, C. L. Gao, D. Qian, Y. Liu, Q.-H. Wang, F.-C. Zhang, Q.-K. Xue, and J.-F. Jia, *Phys. Rev. Lett.* **114**, 017001 (2015).
- [42] H.-H. Sun, K.-W. Zhang, L.-H. Hu, C. Li, G.-Y. Wang, H.-Y. Ma, Z.-A. Xu, C.-L. Gao, D.-D. Guan, Y.-Y. Li, C. Liu, D. Qian, Y. Zhou, L. Fu, S.-C. Li, F.-C. Zhang, and J.-F. Jia, *Phys. Rev. Lett.* **116**, 257003 (2016).
- [43] J. D. Sau, R. M. Lutchyn, S. Tewari, and S. Das Sarma, *Phys. Rev. Lett.* **104**, 040502 (2010).
- [44] J.-S. Xu, K. Sun, Y.-J. Han, C.-F. Li, J. K. Pachos, and G.-C. Guo, *Nat. Commun.* **7**, 13194 (2016).
- [45] B. Huang, C. F. Chan, and M. Gong, *Phys. Rev. B* **91**, 134512 (2015).
- [46] R. Liao, Y. Yi-Xiang, and W.-M. Liu, *Phys. Rev. Lett.* **108**, 080406 (2012).
- [47] S. Nascimbène, *J. Phys. B: At. Mol. Opt. Phys.* **46**, 134005 (2013).
- [48] Z. Fu, L. Huang, Z. Meng, P. Wang, L. Zhang, S. Zhang, H. Zhai, P. Zhang, and J. Zhang, *Nat. Phys.* **10**, 110 (2014).
- [49] Q. Sun, G.-B. Zhu, W.-M. Liu, and A.-C. Ji, *Phys. Rev. A* **88**, 063637 (2013).
- [50] Y. Cao, S.-H. Zou, X.-J. Liu, S. Yi, G.-L. Long, and H. Hu, *Phys. Rev. Lett.* **113**, 115302 (2014).
- [51] Y. Yi-Xiang, J. Ye, and W.-M. Liu, *Phys. Rev. A* **90**, 053603 (2014).
- [52] L. W. Cheuk, A. T. Sommer, Z. Hadzibabic, T. Yefsah, W. S. Bakr, and M. W. Zwierlein, *Phys. Rev. Lett.* **109**, 095302 (2012).
- [53] P. Wang, Z.-Q. Yu, Z. Fu, J. Miao, L. Huang, S. Chai, H. Zhai, and J. Zhang, *Phys. Rev. Lett.* **109**, 095301 (2012).
- [54] Y. Lin, K. Jiménez-García, and I. Spielman, *Nature (London)* **471**, 83 (2011).
- [55] V. Galitski and I. Spielman, *Nature (London)* **494**, 49 (2013).
- [56] J.-Y. Zhang, S.-C. Ji, Z. Chen, L. Zhang, Z.-D. Du, B. Yan, G.-S. Pan, B. Zhao, Y.-J. Deng, H. Zhai, S. Chen, and J.-W. Pan, *Phys. Rev. Lett.* **109**, 115301 (2012).
- [57] S.-C. Ji, J.-Y. Zhang, L. Zhang, Z.-D. Du, W. Zhang, Y.-J. Deng, H. Zhai, S. Chen, and J.-W. Pan, *Nat. Phys.* **10**, 314 (2014).
- [58] Z. Wu, L. Zhang, W. Sun, X.-T. Xu, B.-Z. Wang, S.-C. Ji, Y. Deng, S. Chen, X.-J. Liu, and J.-W. Pan, *Science* **354**, 83 (2016).
- [59] C. Qu, C. Hamner, M. Gong, C. W. Zhang, and P. Engels, *Phys. Rev. A* **88**, 021604(R) (2013).
- [60] C. Hamner, C. Qu, Y. Zhang, J. Chang, M. Gong, C. Zhang, and P. Engels, *Nat. Commun.* **5**, 4023 (2014).
- [61] A. J. Olson, S.-J. Wang, R. J. Niffenegger, C.-H. Li, C. H. Greene, and Y. P. Chen, *Phys. Rev. A* **90**, 013616 (2014).
- [62] J. Li, J. Lee, W. Huang, S. Burchesky, B. Shteynas, F. Top, A. Jamison, and W. Ketterle, *Nature (London)* **543**, 91 (2017).
- [63] J. Li, W. Huang, B. Shteynas, S. Burchesky, F. C. Top, E. Su, J. Lee, A. O. Jamison, and W. Ketterle, *Phys. Rev. Lett.* **117**, 185301 (2016).
- [64] L. Huang, Z. Meng, P. Wang, P. Peng, S.-L. Zhang, L. Chen, D. Li, Q. Zhou, and J. Zhang, *Nat. Phys.* **12**, 540 (2016).
- [65] Z. Meng, L. Huang, P. Peng, D. Li, L. Chen, Y. Xu, C. Zhang, P. Wang, and J. Zhang, *Phys. Rev. Lett.* **117**, 235304 (2016).
- [66] A. Smerzi, S. Fantoni, S. Giovanazzi, and S. R. Shenoy, *Phys. Rev. Lett.* **79**, 4950 (1997).
- [67] J. Sebby-Strabley, M. Anderlini, P. S. Jessen, and J. V. Porto, *Phys. Rev. A* **73**, 033605 (2006).
- [68] C. J. Kennedy, W. C. Burton, C. C. Woo, and W. Ketterle, *Nat. Phys.* **11**, 859 (2015).
- [69] H. Zhai, *Int. J. Mod. Phys. B* **26**, 1230001 (2012).
- [70] X.-J. Liu, *Phys. Rev. A* **91**, 023610 (2015).
- [71] A. P. Schnyder, S. Ryu, A. Furusaki, and A. W. W. Ludwig, *Phys. Rev. B* **78**, 195125 (2008).
- [72] R. Wakatsuki, M. Ezawa, and N. Nagaosa, *Phys. Rev. B* **89**, 174514 (2014).